ISSN 1027-4510, Journal of Surface Investigation: X-ray, Synchrotron and Neutron Techniques, 2021, Vol. 15, No. 1, pp. 128–138. © Pleiades Publishing, Ltd., 2021.
Russian Text © The Author(s), 2021, published in Poverkhnost', 2021, No. 2, pp. 34–44.

Study of the Morphology and Magnetic Properties of Fe Island Films with Antiferromagnetic Layers

L. A. Fomin[a], *, A. V. Chernykh[a], V. A. Berezin[a], and E. A. Vilkov[b]

[a] *Institute of Microelectronics Technology and High Purity Materials, Russian Academy of Sciences, Chernogolovka, Moscow oblast, 142432 Russia*

[b] *Kotelnikov Institute of Radio Engineering and Electronics, Fryazino Branch, Russian Academy of Sciences, Fryazino, Moscow oblast, 141190 Russia*

**e-mail: remagnetization@gmail.com*

Received January 10, 2020; revised March 14, 2020; accepted March 17, 2020

Abstract—Arrays of magnetic nanocontacts are fabricated by growing Fe island films and filling the space between the islands with antiferromagnetic layers. The magnetic structures of the islands and their dependences on their dimensions are studied using atomic-force microscopy and micromagnetic calculations. Micromagnetic numerical calculations of the influence of the spin-polarized current flowing from the ferromagnetic edge into the antiferromagnetic interlayer on magnetization in magnetic antiferromagnet sublattices are carried out. The magnetization skew angle in magnetic antiferromagnet sublattices is found as a function of the current density.

Keywords: atomic-force microscopy, magnetic-force microscopy, micromagnetic calculations, island films, nanocontacts, AFM sublattice skew, spin moment transfer by the current

DOI: 10.1134/S1027451021010237

INTRODUCTION

At present, studies of microstructures and nanostructures made of ferromagnetic (FM) and antiferromagnet (AFM) metals are of interest because of their broad application in spintronics [1–3]. In particular, the study of FM and AFM nanocontacts, through which electric current flows, is important. The authors of [4, 5] showed that, in FM—FM nanocontacts with a spin-polarized current, THz radiation can be generated because of the spin-flip transitions of electrons between subbands with opposite spins in the FM regions. If a rather large potential difference between the nanocontact edges is produced because of a decrease in the transverse nanocontact dimensions or the use of a tunneling interlayer, it is possible to make injected hot electrons enter the upper spin ferromagnet [6]. A rather large current density can lead to the formation of an inverse population in this subband. This offers possibilities for creating a miniature THz source and (in prospect) a laser operating at room temperature on new principles.

Nevertheless, studies in this direction are limited, in particular, by the great difficulty associated with the technology for producing nanocontacts with the use of lithographic methods [7]. In this context, the technology for producing nanocontacts based on the growth of FM metal islands at the stage preceding their percolation is of interest.

The condition for a superhigh density of the spin-polarized current (on the order of 10^9 A/cm^2) required to generate THz radiation in ferromagnet transitions is also a problem [8]. Such a large current density is required to compensate the diffusion current (it reaches 10^{12} A/cm^2 in ferromagnetic metals), which contributes to the leakage of nonequilibrium electrons from the working region and to violation of the condition for THz radiation as a consequence of the radiative energy transitions of electrons with spin flips. In this context, it is interesting to use AFM materials. The authors of [9, 10] showed that the spin-polarized current flowing through the AFM layer can affect its magnetic state, leading to magnetization skew in the magnetic antiferromagnet sublattices. In this case, the current density required to skew the magnetization can be lower by two orders than that required for magnetization reversal of the ferromagnetic layer because of spin moment transfer. The magnetization skew in AFM magnetic sublattices leads to the appearance of the induced magnetic moment and, as a consequence, to spin splitting of the band structure. Thus, the possibility of inversely occupying the upper spin subband in a skewed antiferromagnet and of obtaining THz laser

radiation in the case of a relatively small current appears.

The authors of [11, 12] studied the layered thin-film structure of Pt–AFM with the electrical conduction current in the platinum layer. They called attention (in addition to the skew) to the magnetization rotation in antiferromagnet sublattices caused by the spin current generated in the Pt layer because of conduction-electron scattering in the presence of spin-orbit interaction. They showed that, in such a structure, radiation in the range of 0.5–2 THz can be generated because of nonuniform magnetization rotation in the AFM sublattices.

Another radiation mechanism, namely, the thermal one, makes the creation of a THz source difficult. Near room temperature, the peak of the curve for the radiation absolutely black body is located in the THz frequency range, which is of interest to us. Because the high-density current heats the nanocontact, thermal radiation is generated; its power is comparable with or exceeds that released because of the spin-flip mechanism.

As is seen, creation of a structure in which all necessary processes required for the generation of THz radiation are implemented and (especially) that of the operating THz laser, is a difficult problem. The lack of information about actual electron and magnetic nanocontact structures and about electron-radiation interaction in them makes it difficult to describe the radiation mechanism in the THz range. Therefore, theoretical and experimental studies of arrays of nanocontacts and of their electric, magnetic, and radiative properties manifested during current flow are of interest.

In this paper, we propose the study of FM-metal (Fe) island films on a dielectric (sapphire) substrate as bases for an array of nanocontacts formed after filling of the spaces between the islands with a thin AFM layer. Such an approach makes it possible to obtain large current densities and organize effective heat release from the nanocontact to "massive" well-conducting edges and the substrate. Not the least factor is structure self-organization during its preparation, which simplifies the technology compared with electron-beam lithography usually used for these purposes. The recently actively used method of in situ electrical-resistance monitoring is applied to control the process of growth and the production of island films with desired parameters [13, 14]. In addition, the magnetic properties of FM-metal island films, which can depend on the island dimensions critically [15], have been barely studied using magnetic-force microscopy, which is the reason for these studies in this paper.

EXPERIMENTAL

Fe island films were grown using the method of pulsed laser deposition on heated R-sapphire substrates in high vacuum with in situ control of the film electric resistance. We used a solid-state neodymium-doped yttrium-aluminate laser generating pulses with a wavelength of 0.54 μm in the second harmonic, an energy of 300 mJ, a duration of 10 ns, and a frequency of 1–5 Hz. During the deposition process, the working pressure was at most 10^{-5} Pa in the vacuum chamber with a basic pressure of 10^{-7} Pa. The target irradiation intensity, which slightly exceeded the drip-free evaporation threshold, was 2×10^9 W/cm^2. This provides a constant average deposition rate of 0.6 nm (min Hz) in the case of a constant distance of 5 cm to the substrate.

For two-contact electrical measurements, two low-resistance (on the order of 1 Ω) contact Mo islands with a gap of 1—2 mm, to which elastic contacts made of beryllium bronze were pressed when the sample was placed on a heated table, were deposited onto substrates with dimensions of 5 × 5 mm in advance. The metal was deposited through a narrow gap in a screen covering the sample with the contacts; a film bridge was formed between the contact islands. In this case, the gap width and, accordingly, the bridge width can be decreased to 0.1 mm without the significant influence of edge deposition effects on the bridge width. The electrical resistance of the bridge was measured in real time with digital signal output to a computer with a minimum time step of 1/64 s. For the total growth cycle (up to continuous film formation), the time dependence of the resistance observed in the *in situ* experiments was a comparatively slow decrease (close to linear) in $\log(R(t))$ on the logarithmic scale at a resistance level of 1–10 MΩ ending in a sharp decrease (by three or four orders) corresponding to the percolation transition (Fig. 1a). To produce films consisting of islands with predominantly equiaxial forms, the deposition process was interrupted before the onset of the percolation transition. FeMn and NiO AFM layers were deposited analogously.

The morphology of the grown island films was studied ex situ using scanning electron microscopy (SEM) and atomic-force microscopy (AFM). Typical SEM and AFM images of the island films are shown in Figs. 2a and 2b, respectively. The lateral dimensions and heights of the islands, their forms and the dimensions of the channels between them were determined from the AFM data. The magnetic structure of the islands was studied using magnetic-force microscopy (MFM) in the presence of a magnetic force in the film plane, which was supplied by an external electromagnet. The field induction ranged from –100 to +100 mT and was measured with an accuracy of 0.1 mT. The

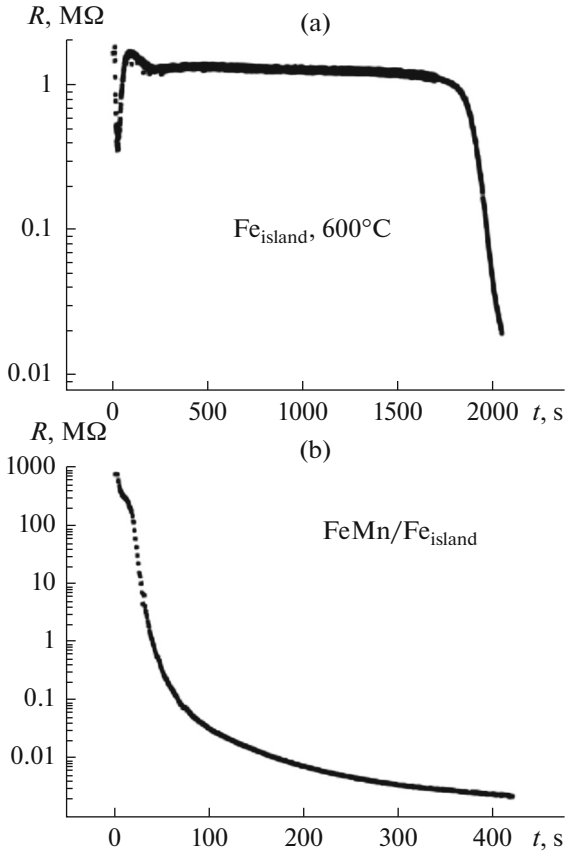

Fig. 1. Characteristic change in the island-film resistance during (a) the growth of Fe islands and (b) the coating of islands with FeMn layers.

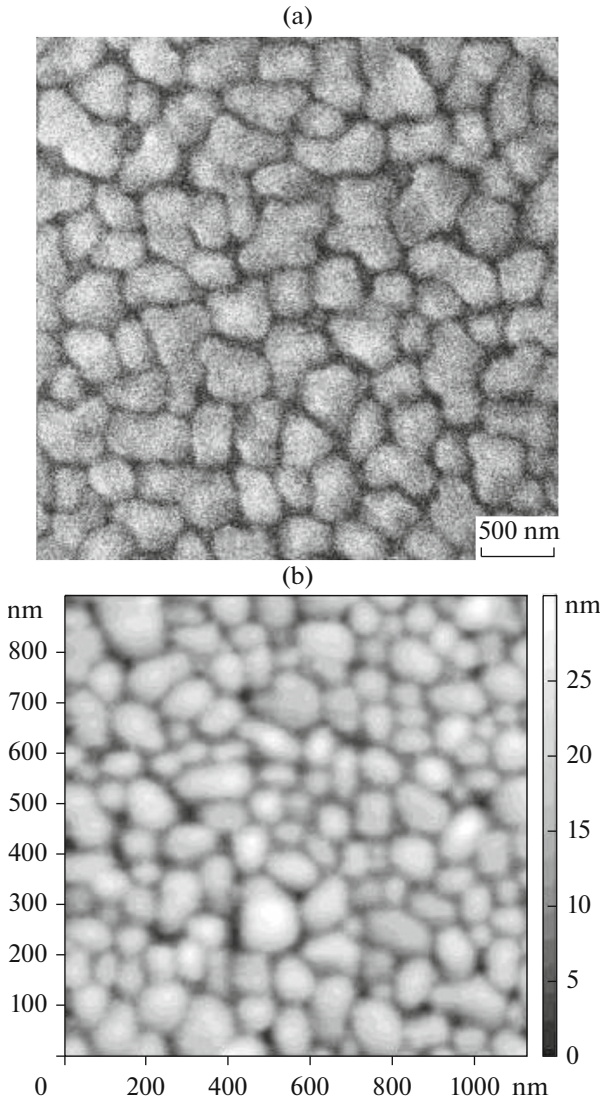

Fig. 2. Typical (a) SEM and (b) AFM images of Fe island films grown by pulsed laser deposition on sapphire.

two-passage procedure was used in the MFM measurements; in this case, during scanning of the sample, the probe measured the surface relief in the first passage, and it was moved away from the surface at a given distance (50 nm) and measured the scattering field of the magnetic sample, following the measured relief. In the first approximation, the probe can be assumed to be a magnetic dipole. In this case, (when using the procedure for measuring the phase of probe oscillations near resonance under the action of the magnetic scattering field of the sample) the phase departure is proportional to the second derivative along the vertical axis z from this field.

As magnetic MFM probes, we used standard cantilevers, which were coated with an Fe film with a thickness of 50 nm deposited by pulsed laser deposition.

MEASUREMENTS

In this paper, we used optimized modes for FM-metal island growth with the minimum saturation of condensation conditions making it possible to move the percolation transition to the range of possibly larger film thicknesses, which is required to control the growth process. High substrate temperatures (500–600°C) and a low average growth rate (a small laser-pulse repetition frequency (1–5 Hz) in our case) corresponded to such requirements. As functions of the chosen growth parameters, Fe island films had different island dimensions (from 0.05 to 1 μm) and heights (from 1 to 200 nm) and widths of the channels of 10—20 nm between the islands. It is seen in the SEM image (Fig. 2a) that the islands are separated, but it was impossible to see islands with dimensions that are 100 nm or less by means of SEM. AFM made it possible to see islands with such dimensions or smaller. However, the gaps between the islands were not resolved in the AFM images (Fig. 2b) if their widths were smaller than the probe point thickness.

Therefore, it is possible to judge whether small-size islands are percolated or not using only their electrical conduction.

The electrical conduction of nonpercolated films had a pronounced nonmetallic temperature dependence, their resistances increased strongly during cooling, reaching 10—100 MΩ at room temperature.

To obtain an array of nanocontacts, the nonpercolated island film was coated with a thin continuous layer of FeMn antiferromagnet with a conductivity that was smaller by an order ($\rho = 150$ μΩ cm) than that of Fe. The AFM layer was deposited on a freshly grown Fe island film without the violation of vacuum after cooling to temperatures below 100°C. The in situ measured resistance of the obtained composite decreased from the initial tens of megaohms to admissible working values (smaller than 1kΩ) for an AFM-layer thickness of several nanometers (Fig. 1b). In such a composite, the current flows predominantly in places with the smallest distances between the islands, which are 10–20 nm in accordance with the SEM measurements. The filling of such FeMn gaps with thicknesses of several nanometers provided conduction channels, whose effective widths can be estimated as 10 nm, at least, for small islands. In the case of experimentally implemented currents up to 100 mA, for samples with working resistances on the order of 1 kΩ and bridge widths of 0.1 mm, a current density of 10^9 A/cm^2 was reached in the individual nanocontact from the total number of parallel contacts in the transverse sample cross-section, whose order was $N = 0.1$ mm/100 nm $= 10^3$.

In addition, it was interesting to compare how the conduction and the behavior of island films coated with an AFM layer with a large resistance, but smaller exchange interaction change in a magnetic field. To do this, the Fe island films were also coated with an AFM NiO layer. After cooling the islands to 100°C, a NiO film with a thickness of 20 nm was deposited onto the sample; it was synthesized with a rate of 2.5 nm/min by evaporation from a pure Ni target in the presence of oxygen with a pressure of 10^{-1} Pa and was continuous and homogeneous in accordance with the AFM data and electrical measurements. The resistance of the cooled Fe island film was on the order of 100 MΩ and was almost the same during oxygen puffing and NiO deposition; i.e., nickel was oxidized completely during evaporation; in this case, the Fe islands were not oxidized in the NiO synthesis process.

The crystal structure of Fe island films was not studied in this paper; however, if the fact that the used growth temperatures (500–600°C) were significantly higher than those successfully used for the diffusion ordering of Fe thin layers (usually 300–400°C, for example, [16]) is taken into account, then it is possible to assume that each individual island is one crystallite. As for their crystallographic orientation and possible epitaxy on the sapphire *R*-plane, the cubic faceting of the Fe islands corresponding to the known epitaxial orientation of body-centered cubic (bcc) metals on R-sapphire $Fe(001)\|Al_2O_3(\bar{1}012)$, $Fe[110]\|Al_2O_3[11\bar{2}0]$, $Fe[\bar{1}10]\|Al_2O_3[1\bar{1}01]$ was observed reliably on the AFM images of films grown at 600°C. For islands grown at 500°C, the faceting was not a characteristic feature, which makes it impossible to conclude that their structures are epitaxial.

The result that the NiO films obtained by the above method have antiferromagnetic properties was shown in previously conducted experiments on NiO/Ni sandwich structures demonstrating an exchange shift [17] of the hysteresis loop in such samples. The exchange shift was also observed previously for FeMn/Fe structures, which is evidence that FeMn films are antiferromagnetic [18].

The results of measuring the THz radiation spectra for a series of samples, through which the current flowed, were published in part in the conference papers [19, 20] and are planned to be published in a subsequent paper.

CALCULATION PROCEDURE

We calculated the magnetic structure of the Fe islands using AFM data on their dimensions and forms. To calculate the distribution of the lattice magnetization and to find its time evolution in an effective magnetic field, we used the Landau–Lifshitz equation (1).

$$\frac{\partial \mathbf{M}}{\partial t} = -\gamma \mathbf{M} \times \mathbf{H}_{\text{eff}} - \frac{\alpha\gamma}{|\mathbf{M}|} \mathbf{M} \times \mathbf{M} \times \mathbf{H}_{\text{eff}}, \quad (1)$$

$$H_{\text{eff}} = -\frac{\delta E}{\delta M} + H_{sd}, \quad (2)$$

where E is the free energy of the ferromagnet volume unit, $\mathbf{M}$ is the magnetization of the ferromagnet volume unit, γ is the gyromagnetic ratio, α is the attenuation parameter, $\mathbf{H}_{\text{eff}}$ is the effective field, and $\mathbf{H}_{\underline{sd}}$ is the effective field of the *s–d* exchange interaction between the conduction-electron spins and lattice atoms. The effective field is defined as the variational derivative of the free energy with respect to the magnetic moment (2). In this paper, the OOMMF program [21], which uses the finite difference method to solve equations in partial derivatives, was used.

The magnetic structure of the islands was calculated for their dimensions and forms taken from actual AFM measurements. Namely, from the file obtained as a result of AFM scanning of the island-film surface region, using the "octave" packet [22], we created an input file for the OOMMF program, in which a three-

dimensional array of data on the magnetic material magnetization in each calculation cell was contained. The island magnetization was zero above the island surface and was the same as for Fe below that. The magnetization direction was given as constant along the axis x in each island. Then in the evolution process, the magnetization distribution was varied until it became equilibrium, in accordance with Eq. (1). The MFM image was simulated from the calculated equilibrium distribution of the magnetization.

As is known, the OOMMF program is intended for calculation of the magnetic structures of ferromagnets. However, it can also be used to calculate antiferromagnetic structures in some cases. If the cell is taken to be rather small (so that only one atom is contained in it), then a two-sublattice antiferromagnet can be modeled by specifying the exchange-interaction constant A as negative, as was done in [23]. In this case, the expression for the anisotropy energy remains the same, and the magnetostatic interaction can be neglected for small sample dimensions.

The magnetic structures of $Fe_{50}Mn_{50}$ and NiO have been studied in many papers. As for $Fe_{50}Mn_{50}$, in the majority of papers, it was concluded that the magnetic moments of atoms are directed along the $\langle 111\rangle$ cubic directions in the bcc-type lattice of this alloy [24, 25]. However, in this case, it was (mainly) assumed that the $Fe_{50}Mn_{50}$ alloy is ordered, although not necessarily, and Fe atoms can occupy the places of Mn atoms. There also exist models in which the magnetic moments are located along the $\langle 100\rangle$ directions, which were discussed, for example, in [25].

In this paper, we used a simplified model of an antiferromagnet with two sublattices. In spite of the fact that this model is rough, we assumed it to be quite justified, because the number of sublattices does not affect the physics of the process of the interaction between the current and the sublattice magnetization. In accordance with [11, 12], an effective magnetic field $\mathbf{H}_{sd}$ was produced in the antiferromagnet as a result of spin injection by the current; it was caused by the s–d exchange interaction between injected electrons and d electrons of lattice atoms and led to magnetization skew of the magnetic sublattices of the antiferromagnet. This effective field can be decomposed into two components; one (3) is parallel to the induced magnetization (injected one) and another (4) is perpendicular to it (of the Slonczewski—Berger type).

$$\mathbf{H}_{||} = \frac{\tau_{sf} P \mu_B}{\tau_{sd} \gamma e L_{AFM} M_s} j \hat{\mathbf{M}}_F, \quad (3)$$

$$H = \frac{P \mu_B}{\gamma e L_{AFM} M_s} j \hat{M} \times \hat{M}_F, \quad (4)$$

where $\tau_{sf} = 1 \times 10^{-12}$ s is the spin relaxation time; $\tau_{sd} = (\alpha_{sd}\gamma M_s)^{-1} = 10^{-15}$ s is the s–d exchange time, which is expressed in terms of the s–d exchange constant $\alpha_{sd} \sim 10^4$; $\gamma = 2.211 \times 10^5$ (A/m)$^{-1}$ s^{-1} is the gyromagnetic ratio; and $M_s = 800 \times 10^3$ A/m is the antiferromagnet-sublattice saturation magnetization. $P = 0.5$ is the degree of current polarization, j is the current density, e is the elementary charge, L_{AFM} is the antiferromagnet thickness, μ_B is the Bohr magneton, $\hat{\mathbf{M}}$ is the unit vector in the direction of induced antoferromagnet magnetization, and $\hat{\mathbf{M}}_F$ is the unit vector in the ferromagnet magnetization direction.

Using the OOMMF program with an additionally written module for inclusion of the influence of the spin-polarized current, we calculated the evolution of the magnetic structure of the FM/AFM structure in the form of two FM edges and a thin AFM interlayer between them when the current flows. The geometry of the calculation model is shown in Fig. 3. The interlayer thickness was taken to be 10 nm. The calculation-cell size was approximately equal to the interatomic distance, $\Delta x = \Delta y = \Delta z = 0.4$ nm. Because we were interested in the influence of the current only on the antiferromagnet, the magnetic moments in the FM edges were taken to be constant in the calculation. This made it possible to simplify the problem and decrease the calculation time. The current flowed in the direction x and was polarized along x (along the FM magnetization). The current density and polarization were the same in space. In the AFM, the magnetic moments of atoms were located initially along axis y (perpendicularly to the FM magnetization) and were directed oppositely to one another in neighboring calculation cells. For the Fm edges, we used the same Fe parameters as tacitly taken in the OOMMF program, and the FeMn parameters were taken from [23] for the AFM interlayer. The exchange constants were $A_{Fe} = 21 \times 10^{-12}$ J/m for Fe and $A_{FeMn} = -3 \times 10^{-12}$ J/m for FeMn. The interlayer exchange constant in the Fe/FeMn interface was taken as A_{Fe}. The anisotropy was assumed to be cubic and the same in the entire structure with the positive constant $K_1 = 48 \times 10^3$ J/m^3 (the easy magnetization axes were located along the cube edges). Such anisotropy corresponds to Fe growth on the sapphire R-plane, as was studied in our previous papers [26, 27]. The saturation magnetization was taken as $M_s = 1700 \times 10^3$ A/m for Fe, and it was $M_s = 800 \times 10^3$ A/m for the FeMn sublattices.

RESULTS AND DISCUSSION

The magnetization distribution in islands with lateral dimensions of about 50 nm was calculated using the micromagnetism method. The AFM image and

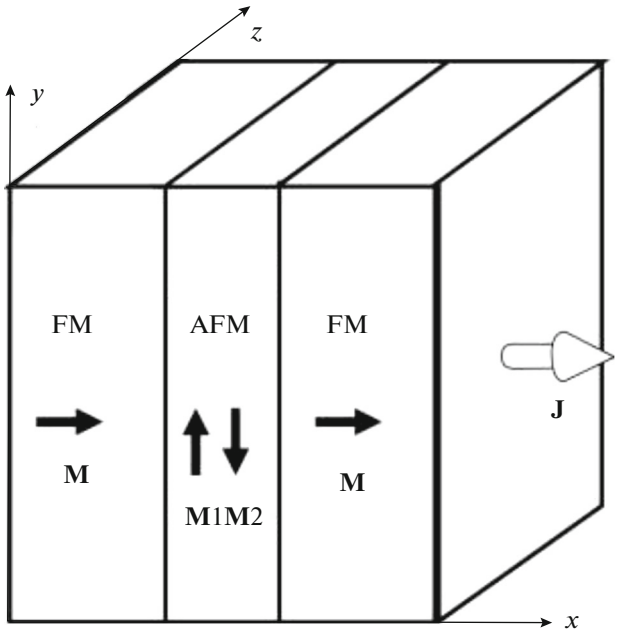

Fig. 3. Geometry of the calculation model of the influence of the spin-polarized current on the Fe/FeMn magnetic structure in the form of two Fe edges and a thin FeMn interlayer between them. The black arrows show the directions of the magnetization vectors **M** in the ferromagnet and the antiferromagnet sublattices $\mathbf{M}_1$ and $\mathbf{M}_2$. The white arrow shows the current direction.

the MFM contrast modeled by means of it are shown in Fig. 4. The arrows show the magnetization direction in the film plane. The calculation showed that the magnetization vector goes slightly out of the plane. It is seen that the magnetization distribution is nonuniform in each individual island, and the magnetization of neighboring islands affect it.

Figure 5 shows the AFM image of the surface and the experimentally measured MFM contrast of Fe islands coated with an FeMn film in an external magnetic field. The lateral island dimensions were about 1 μm, and their heights were about 250 nm. The MFM measurements showed that the islands behaved as individual magnets at such dimensions. Their magnetic structures depended weakly on the environment. The dimensions of the characteristic features in the MFM contrast corresponded to those of the islands. The magnetic structures of the islands varied in small fields (on the order of 1 mT) and barely changed as the field continued to increase. At the same time, the characteristic features in the MFM contrast exceeded the island dimensions noticeably for small island dimensions (on the order of 100 nm). The MFM measurements in an external magnetic field made it possible to state that the small islands are related to each other magnetically. Figure 6 shows the AFM and MFM images of Fe islands coated with a NiO film.

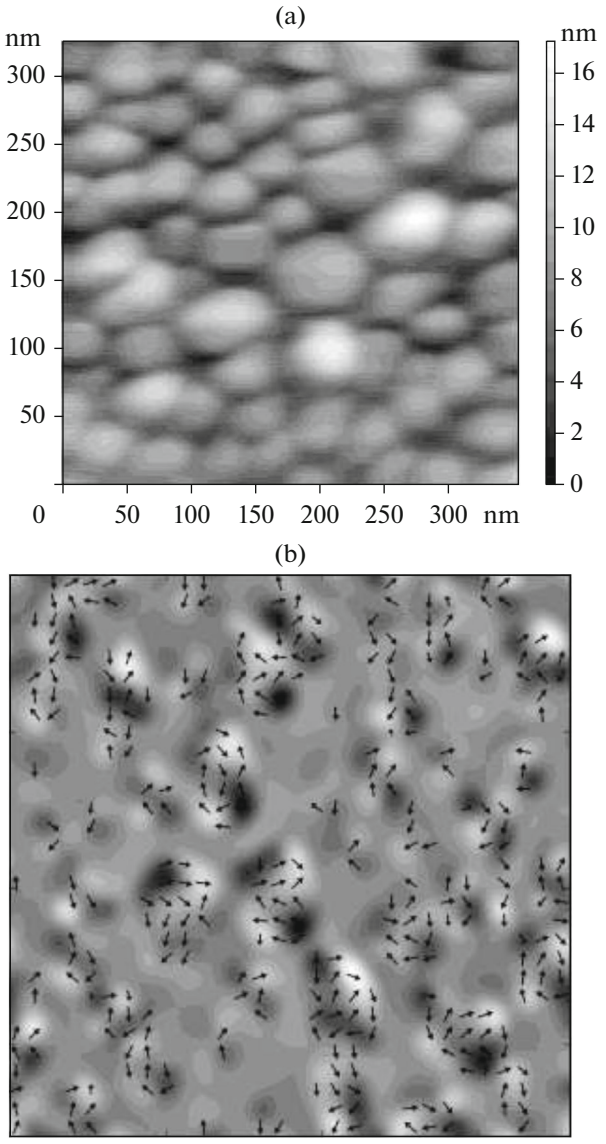

Fig. 4. (a) AFM image of the island film and (b) the modeled MFM contrast of the islands. The arrows show the local magnetization direction in the film plane.

The island size was approximately 100 nm (Fig. 6a), but the size of the characteristic feature in the MFM image was approximately 500 nm. This means that the islands are related to each other magnetically. The thin NiO antiferromagnet interlayer did not weaken the interaction between islands noticeably. an external magnetic field with an induction of −56 mT was applied to the sample, then the field was decreased gradually to zero, and then was increased gradually to +56 mT. When the field was varied from −56 mT (Fig. 6b) to zero (Fig. 6c) and then to +8 mT, the MFM contrast of the sample changed weakly. Then it changed sharply in a field of about 8 MT (Fig. 6d), and it continued to vary up to 30 mT with increasing field

(Fig. 6e). It is likely that the sample coercive force was approximately 8 mT, and the saturation field was about 30 mT.

To study the skew of the antiferromagnet lattices, we used the above calculation procedure. Current densities ranging from $j = 2 \times 10^5$ A/cm^2 to $j = 2 \times 10^9$ A/cm^2 were taken in the calculation. The calculation results are shown in Figs. 7 and 8. In the evolution process, in accordance with Eq. 1, the system made the transition from the initial state (Fig. 7a) to the steady state (Fig. 7b) at a current density of $j = 2 \times 10^5$ A/cm^2 and to the state shown in Fig. 7d at a higher current density of $j = 1 \times 10^9$ A/cm^2. The intermediate system state is shown in Fig. 7c. Thus, for high current densities, the rotation of the antiferromagnet sublattice magnetization is nonuniform, which can lead to the generation of THz radiation in accordance with the mechanism described in [11, 12]. The antiferromagnet sublattices collapsed at current densities j of 2×10^9 A/cm^2 or more. The evolution of the m_x, m_y, and m_z magnetization components of the entire structure at $j = 1 \times 10^9$ A/cm^2 is shown in Fig. 8. In the initial state ($t = 0$), the m_x component of the structure magnetization was determined by the ferromagnetic edges, and the m_z and m_y components were zero. When the current flowed, the sublattice magnetization vectors began to rotate about the direction x, and their x components increased. First, the magnetic moments of the antiferromagnet atoms rotated noncoherently (Fig. 7c), then this rotation became more coherent and gradually decayed. The rotation frequency and its decay rate were proportional to the current density. At $j = 1 \times 10^9$ A/cm^2 (Fig. 8), the rotation frequency was approximately 5 THz. This frequency value was several times larger than the maximum frequency obtained in [11, 12]; however, the current density in this calculation was also very large. The frequency of magnetic-moment rotation was 0.5 THz for a current of $j = 1 \times 10^8$ A/cm^2, which was close to the minimum frequency in these papers. After a certain time, the magnetic moments of antiferromagnet lattice atoms were arranged in the xy plane, as is shown in Fig. 7d. The sine of the skew angle can be obtained from the final average value of the m_x component of the magnetization vector. In the range from the critical current ($j = 1 \times 10^8$ A/cm^2) to the sublattice collapse current ($j = 1 \times 10^{10}$ A/cm^2), it was proportional to the current density (Fig. 9a).

The obtained current densities that are required to skew the antiferromagnet, were larger than those calculated in [9]. It is probable that this was related to the large anisotropy energy and the strong interlayer exchange interaction with Fe, which were used in this paper.

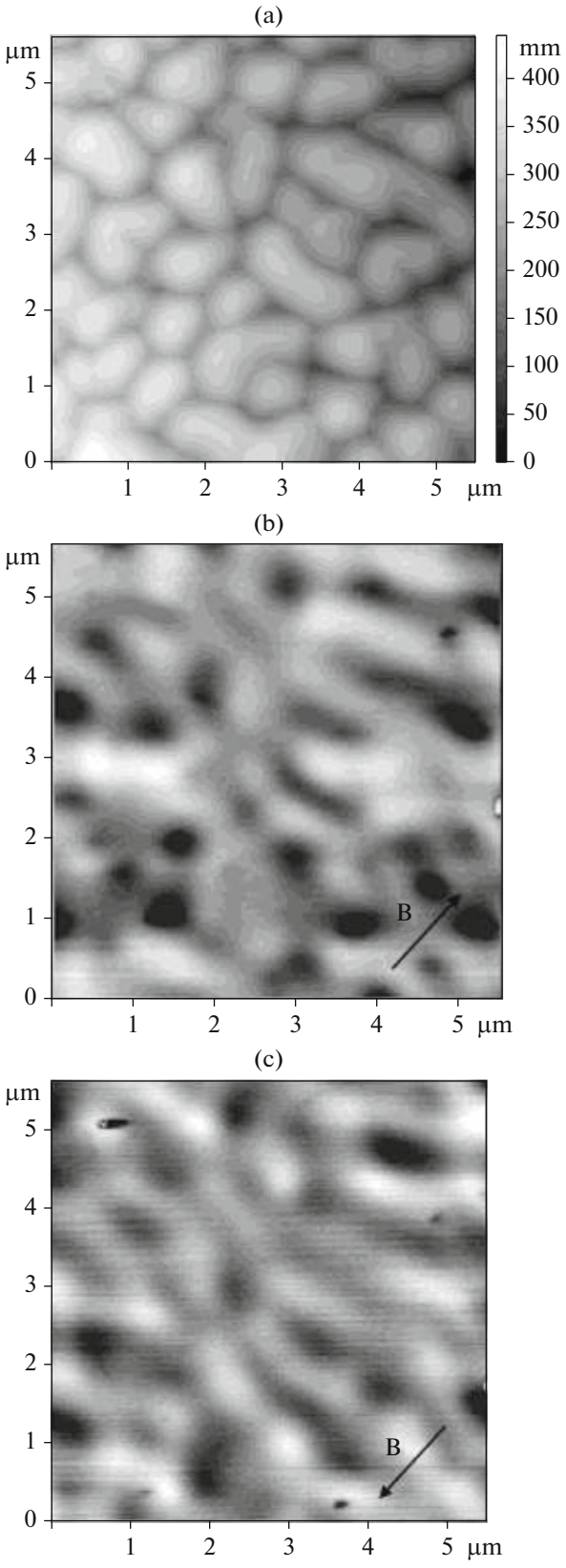

Fig. 5. (a) AFM and MFM images of Fe islands coated with an FeMn film in an external magnetic field with inductions of (b) 67 and (c) 56 mT. The field direction is shown by the arrow.

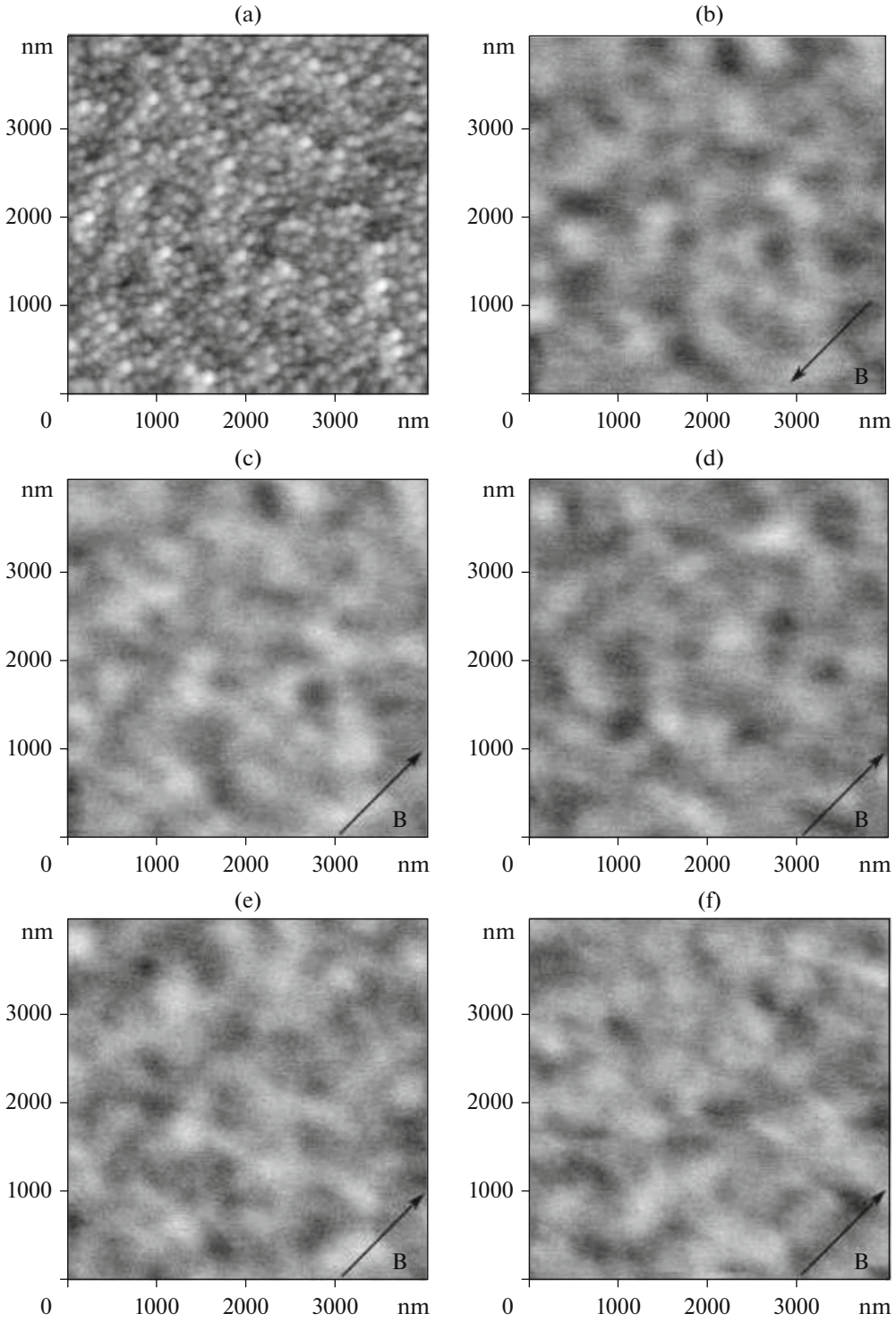

Fig. 6. (a) AFM and MFM images of Fe islands coated with a NiO film in an external magnetic field with inductions of (b) 56, (c) 0, (d) 8, (e) 30, and (f) 56 mT. The field direction is shown by the arrow.

The authors of [9] suggested that the sublattice magnetization direction in the AFM must be primarily perpendicular to the magnetization in the FM. If, as the initial conditions, it is taken that the sublattice magnetization direction in the AFM is collinear to the magnetization in the FM (along the axis x), then, in accordance with the calculation, the system will make the transition to an analogous final state (Fig. 7d), evolv-

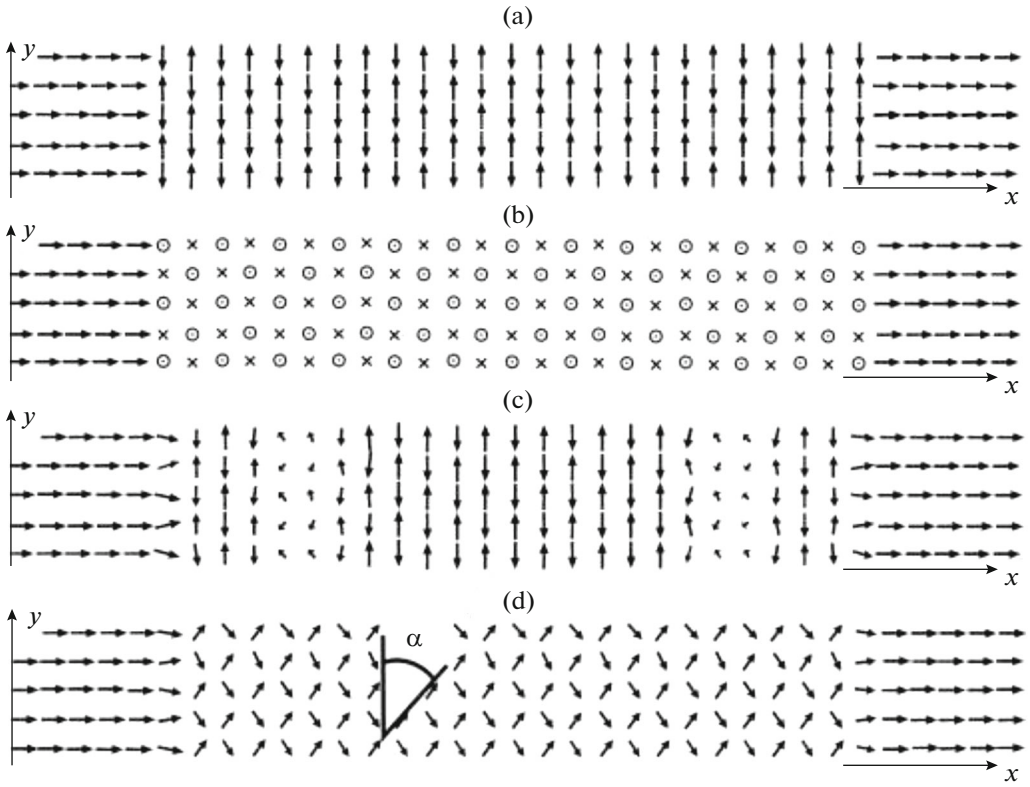

Fig. 7. (a) Initial state in the calculation model, (b) the final state for a current density of 2×10^5 A/cm^2, (c) the result of evolution at 2×10^{-13} s and a current density of 1×10^9 A/cm^2, and (d) the final state for a current density of 1×10^9 A/cm^2 .

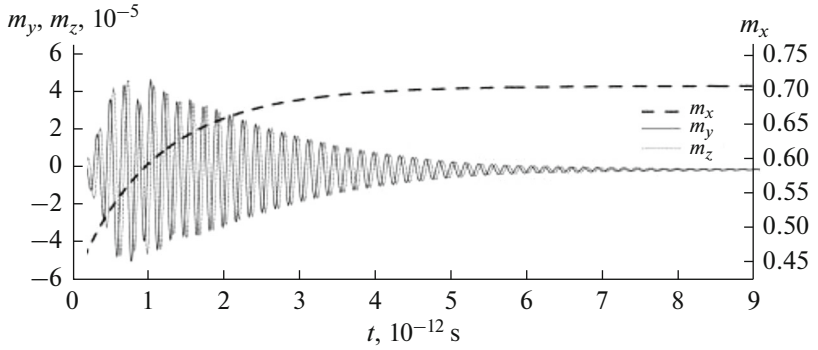

Fig. 8. Evolution of the m_x component and also m_y and m_z components of the dimensionless (normalized to unity) magnetic moment of the entire system for a current density of 1×10^9 A/cm^2.

ing in time in a more complicated way when the current having a rather high density ($j = 1 \times 10^9$ A/cm^2) and polarized along the axis x flows.

For comparison, we calculated the effect of a strong magnetic field on the antiferromagnet magnetization. We considered a sample with dimensions of $10 \times 8 \times 8$ nm in the case of the direction of the AFM sublattice magnetization along axis y. A magnetic field was applied along the axis x. The dependence of the skew angle on the magnetic-field induction is given in Fig. 9b. It is seen that the sine of the skew angle is 2×10^{-4} for a field with an induction of 0.1 T. The antiferromagnet lattice was barely skewed if a field with an induction of up to 10 T was applied along the axis y (along the antiferromagnet sublattice magnetization).

CONCLUSIONS

We have proposed a procedure for fabricating arrays of magnetic nanocontacts made of FM metals with AFM interlayers; it was based on the controlled

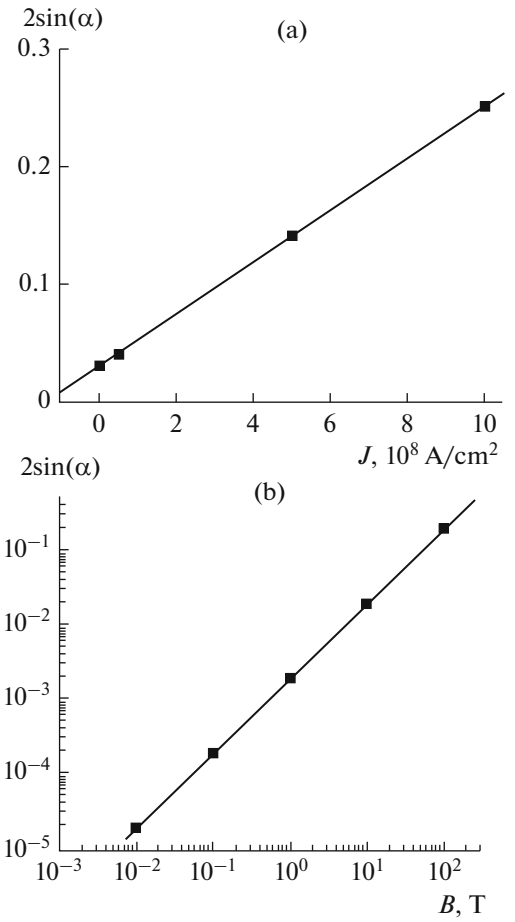

Fig. 9. Dependence of the doubled sine of the magnetization (m_x) skew angle on (a) the spin-polarized current density and (b) the external magnetic field.

growth of island films. The developed technology combined pulsed laser deposition, in situ monitoring of the electrical resistances, and ex situ AFM and SEM characterization of the films. In the optimum modes, namely, at high temperatures (400-600°C) and low laser-pulse repetition frequencies (1–5 Hz), we have obtained island Fe films with different island dimensions from 0.05 to 1 μm, heights from 1 to 200 nm, and widths of 10–20 nm of channels between the islands, which were the objects under study.

Using methods of MFM and micromagnetic calculations, we have studied the magnetic structures of Fe islands and their dependence on their dimensions and the external field. It was shown that, for small island dimensions (100 nm or less), the characteristic features in the MFM contrast exceeded the island dimensions noticeably, and collective magnetic states were observed. On the other hand, for large island dimensions (on the order of several micrometers), the magnetic structure was determined by the island properties. We obtained quantitative estimates of the influence of the spin-polarized current flowing in the AFM interlayer from the FM edge on the skew of its sublattice magnetization. The calculations showed that the sine of the magnetization skew angle depended linearly on the current density and reached a value of ≈0.125 for a current density of 10^9 A/cm^2. The obtained results can be useful for the interpretation of emission spectra of radiators based on Fe/FeMn island films in the THz range.

FUNDING

The work was supported by State Program no. 007-00220-18-00. E. A.Vilkov is grateful to the Russian Foundation for Basic Research (project no. 18-57-76001 ERA_a).

REFERENCES

1. V. Baltz, A. Manchon, M. Tsoi, et al., Rev. Mod. Phys. **90**, 015005 (2018). https://doi.org/10.1103/RevModPhys.90.015005
2. S. S. Dhillon, et al., J. Phys. D: Appl. Phys. **50**, 043001 (2017). https://doi.org/10.1088/1361-6463/50/4/043001
3. F. Hellman, et al., Rev. Mod. Phys. **89**, 025006 (2017). https://doi.org/10.1103/RevModPhys.89.025006
4. A. M. Kadigrobov, Z. Ivanov, T. Claeson, et al., Europhys. Lett. **67**, 948 (2004). https://doi.org/10.1209/epl/i2004-10159-8
5. A. M. Kadigrobov, R. I. Shekhter, and M. Jonson, Low Temp. Phys. **38**, 1133 (2012). https://doi.org/10.1063/1.4770510
6. A. M. Kadigrobov, R. I. Shekhter, S. I. Kulinich, et al., arXiv:1101.2862, 2011. https://doi.org/10.1088/1367-2630/13/2/023007
7. V. Korenivski, A. Iovan, A. M. Kadigrobov, and R. I. Shekhter, Europhys. Lett. **104**, 27011 (2013). https://doi.org/10.1209/0295-5075/104/27011
8. Yu. V. Gulyaev, P. E. Zil'berman, A. I. Panas, et al., J. Commun. Technol. Electron. **55**, 668 (2010).
9. Yu. V. Gulyaev, P. E. Zil'berman, and E. M. Epshtein, J. Exp. Tech. Phys. **114**, 296 (2012).
10. Yu. V. Gulyaev, P. E. Zil'berman, and E. M. Epshtein, J. Commun. Technol. Electron. **57**, 329 (2012).
11. R. Khymyn, I. Lisenkov, V. Tiberkevich, et al., Sci. Rep. **7**, 43705 (2017). https://doi.org/10.1038/srep43705
12. O. R. Sulymenko, O. V. Prokopenko, V. S. Tiberkevich, et al., Phys. Rev. Appl. **8**, 064007 (2017). https://doi.org/10.1103/PhysRevApplied.8.064007
13. N. Abdellaoui, A. Pereira, M. Novotny, et al., Appl. Surf. Sci. **418**, 517 (2017).
14. J. S. Agustsson, U. B. Arnalds, A. S. Ingason, et al., Appl. Surf. Sci. **254**, 7356 (2008).
15. C. Martínez Boubeta, C. Clavero, J. M. García-Martín, et al., Phys. Rev. B: Condens. Matter Mater. Phys. **71**, 014407 (2005).

16. M. Bowen, V. Cros, F. Petroff, et al., Appl. Phys. Lett. **79**, 1655 (2001). https://doi.org/10.1063/1.1404125
17. W. H. Meiklejohn, J. Appl. Phys. **33**, 1328 (1962). https://doi.org/10.1063/1.1728716
18. G. M. Mikhailov, A. V. Chernykh, and L. A. Fomin, Materials **10**, 1156 (2017). https://doi.org/10.3390/ma10101156
19. L. A. Fomin et al., in *Proceedings of the XVII All-Russian Sukhorukov School-Seminar "Physics and Application of Microwaves," Moscow, 2019*, (Mosk. Gos. Univ., Moscow, 2019), p. 14.
20. V. G. Krishtop et al., in *Proceedings of the XXII International Symposium "Nanophysics and Nanoelectronics"* (Nizhegor. Gos. Univ. im. N.I. Lobachevskogo, Nizhny Novgorod, 2018), Vol. 1, p. 208.
21. The Object Oriented MicroMagnetic Framework (OOMMF) Project at ITL/NIST. https://math.nist.gov/oommf/.
22. GNU Octave. https://www.gnu.org/software/octave/.
23. N. N. Phuoc and T. Suzuki, J. Appl. Phys. **101**, E501 (2007). https://doi.org/10.1063/1.2668167
24. R. D. Hempstead, S. Krongelb, and D. A. Thompson, IEEE Trans. Magn. **14**, 521 (1978). https://doi.org/10.1109/TMAG.1978.1059838
25. M. Ekholm and I. A. Abrikosov, Phys. Rev. B: Condens. Matter Mater. Phys. **84**, 104423 (2011). https://doi.org/10.1103/PhysRevB.84.104423
26. G. M. Mikhailov, L. A. Fomin, V. Yu. Vinnichenko, et al., Solid State Phenom. **168–169**, 300 (2010). doi 10.4028/www.scientific.net/SSP.168-169.300
27. L. A. Fomin, V. Yu. Vinnichenko, I. V. Malikov, and G. M. Mikhailov, J. Magn. Magn. Mater. **330**, 6 (2013). https://doi.org/10.1016/j.jmmm.2012.08.001

Translated by L. Kulman